Intermixing of ordinary and anomalous Hall effect in $SrRuO_3$

Debangsu Roy,[1] Noam Haham,[1] James W. Reiner,[2] Efrat Shimshoni,[1] and Lior Klein[1]

[1]*Department of Physics, Nano-magnetism Research Center, Institute of Nanotechnology and Advanced Materials, Bar-Ilan University, Ramat-Gan 52900, Israel*

[2]*HGST, a Western Digital Company, San Jose, California 95135, USA*

(Received 21 June 2015; revised manuscript received 7 October 2015; published 1 December 2015)

The Hall effect resistivity ρ_{xy} of high-quality films of the itinerant ferromagnet $SrRuO_3$ was measured at low temperatures. $SrRuO_3$ films have large uniaxial magnetocrystalline anisotropy, and in the relevant temperature range the easy axis is 30° degrees from the film normal. We measure changes in ρ_{xy} associated with changes in the orientation of the magnetization (**M**) for the same applied magnetic field **B** [$\Delta\rho_{xy}(\mathbf{B},\Delta\mathbf{M})$], and we find that with increasing **B**, $\Delta\rho_{xy}(\mathbf{B},\Delta\mathbf{M})$ changes its sign and its magnitude becomes more than an order of magnitude larger than the remanent (spontaneous) anomalous Hall effect. Furthermore, it appears that ρ_{xy} cannot be described as a sum of a term that depends on **B** and a term that depends on **M**, that is, the ordinary Hall effect and the anomalous Hall effect are effectively intermixed. We address qualitatively a possible link between the observed behavior of ρ_{xy} and the predicted existence of Weyl nodes in $SrRuO_3$.

DOI: 10.1103/PhysRevB.92.235101 PACS number(s): 75.47.−m, 72.25.Ba, 73.50.−h, 75.75.Cd

I. INTRODUCTION

Some of the most exciting condensed-matter systems exhibit electrical transport phenomena determined by topological features of the bands. Such phenomena include the quantum Hall effect and the intriguing features of the more recently discovered topological insulators [1]. Among the different topological states, the state known as Weyl metal has attracted considerable interest [2]. Weyl nodes in the electronic band structure are Dirac points in momentum space, characterized by a topological charge, which appear in pairs. They are particularly interesting when they occur in band structures of magnetic metals. In such cases, their existence is expected to be manifested by their considerable effect on the anomalous Hall affect (AHE) [3] via the Berry phase mechanism.

The AHE appears in magnetic conductors in association with the magnetization (**M**), as part of the total Hall effect (HE), and in addition to an ordinary Hall effect (OHE) contribution, associated with the magnetic field (**B**). The HE gives rise to transverse resistivity ρ_{xy}, which is antisymmetric in **B** and **M**. Commonly, ρ_{xy} is presented as a sum of two independent contributions associated with the OHE and the AHE: $\rho_{xy} = R_0 B_\perp + \rho_{xy}^{\mathrm{AHE}}$. Here, R_0 is the OHE coefficient and $B_\perp$ is the component of the applied magnetic field in the z direction. The form of the AHE contribution ρ_{xy}^{AHE} depends on the mechanism responsible for the AHE. Extrinsic models [4,5] correlate the AHE to antisymmetric scattering processes, and the contribution is expressed as $\rho_{xy}^{\mathrm{AHE}} = R_s \mu_0 M_\perp$, where R_s is the AHE coefficient, given by $R_s = a\rho_{xx} + b\rho_{xx}^2$, and $M_\perp$ is the component of magnetization in the z direction. The linear term in ρ_{xx} of R_s is attributed to skew scattering [4], whereas the quadratic term in ρ_{xx} is correlated with the side jump mechanism [5].

In the theoretical framework proposed by Karplus and Luttinger [6], ferromagnetic conductors also exhibit intrinsic AHE related to the topological properties of the band. In such models, the dependence of the AHE on magnetization is due to the interplay between **M** and the band structure [7,8]. This mechanism is commonly referred to as the Berry phase mechanism, and its contribution to the AHE takes the form $-\rho_{xx}^2 \sigma_{xy}(\mathbf{M})$. The Berry phase mechanism links topological features of the band to the AHE resistivity, which makes the AHE a useful tool for studying the manifestation of intriguing topological features, including the existence of Weyl nodes.

The AHE in $SrRuO_3$, which is an itinerant ferromagnet, has attracted considerable interest [9–13]. According to several theoretical calculations, Weyl nodes (pairs of Dirac points in momentum space) occur in the band structure of $SrRuO_3$ and are expected to make a significant contribution to the AHE in this compound [9–11]. One of these reports [9] has attributed the nonmonotonic temperature dependence of the AHE in $SrRuO_3$ (see Fig. 1) to the existence of magnetic monopoles in momentum space (essentially, this is an analogous term for the topological structure imposed by Weyl nodes). Others have claimed that this behavior can also be explained by assuming an extrinsic positive contribution to ρ_{xy} associated only with the side jumps mechanism with an intrinsic negative contribution to ρ_{xy} associated with Berry phase contributions [12]. According to this scenario, the Berry phase mechanism dominates at low ρ_{xx}; however, it is suppressed with increasing ρ_{xx} due to band smearing effects associated with the carrier scattering time. This scenario was supported by demonstrating the scaling of the AHE with ρ_{xx} for $SrRuO_3$ films with a wide range of resistivities (controlled by film thickness) and in a wide range of temperatures, including both the ferromagnetic and paramagnetic phases.

As discussed below, the contribution of Weyl nodes to the AHE is expected to depend on both **B** and **M**. Consequently, changes in ρ_{xy} associated with changes in **M** may in principle be much larger than the zero field ρ_{xy}^{AHE}. Furthermore, since the AHE is directly affected by **B** (and not merely due to its effect on **M**), effective intermixing of the AHE and the OHE is expected.

The Weyl node contribution is part of the intrinsic Berry phase contribution to the AHE; therefore, it will be manifested in the clearest way if extrinsic sources to AHE are suppressed as much as possible. Therefore, in trying to identify Weyl node contributions to the AHE in $SrRuO_3$, we have used thin films of $SrRuO_3$ with exceptionally low residual resistivity and measured the AHE at low temperatures. We measured

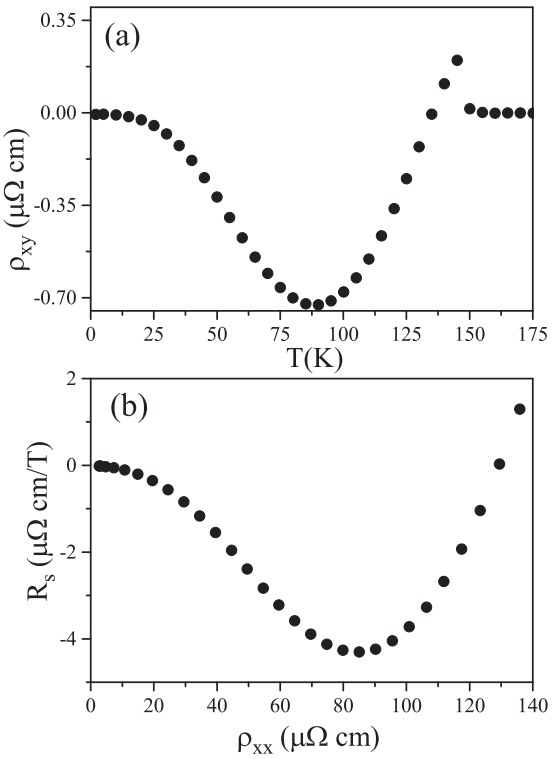

FIG. 1. (a) The spontaneous AHE vs temperature. (b) The AHE coefficient (R_s) vs ρ_{xx}.

changes in ρ_{xy} associated with changes in **M** for the same **B** [$\Delta\rho_{xy}(\mathbf{B},\Delta\mathbf{M})$], and we found that with increasing **B**, $\Delta\rho_{xy}(\mathbf{B},\Delta\mathbf{M})$ changes its sign and its magnitude becomes more than an order of magnitude larger than the zero field ρ_{xy} with **M** in its remanent state (the spontaneous AHE). Furthermore, it appears that ρ_{xy} cannot be described as a sum of a term that depends on **B** and a term that depends on **M**, which means that the OHE and the AHE are effectively intermixed.

We find our results to be qualitatively consistent with the predicted existence of Weyl nodes in $SrRuO_3$ and the expected striking effect of this intriguing topological state on electrical transport properties.

II. EXPERIMENTAL DETAILS

Our samples are epitaxial $SrRuO_3$ thin films grown on slightly miscut (∼2°) substrates of $SrTiO_3$ by reactive electron beam evaporation. The films are untwinned orthorhombic single crystals with lattice parameters of $a \cong 5.53$, $b \cong 5.57$, and $c \cong 7.85$ Å. The Curie temperature T_C of these films is ∼150 K and they exhibit an intrinsic uniaxial magnetocrystalline anisotropy where the anisotropy field in the low-temperature limit is more than ∼7 T [14]. The easy axis varies in the (001) plane between 45° from the film normal at T_C to 30° in the low-temperature limit (2 K) [15,16]. The films have been patterned using photolithography for transverse and longitudinal resistivity measurements, which were carried out in Quantum Design PPMS-9. Symmetric and antisymmetric signals were separated using the common method of exchanging the voltage and the current leads [17].

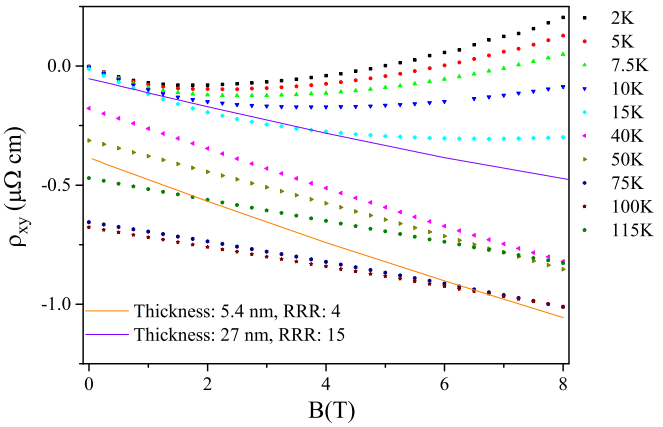

FIG. 2. (Color online) Hall resistivity as a function of the magnetic field at several temperatures (indicated in the legend) applied along the easy axis. The continuous lines are for two other films with a lower resistivity ratio at 10 K.

The measurements presented here are for a 90-nm-thick film that exhibits an exceptionally high residual resistivity ratio (RRR) of ∼90, signifying an outstanding quality. The temperature dependence of the zero-field ρ_{xy}^{AHE} and the extracted dependence of R_s (obtained by dividing ρ_{xy} by $M_\perp$) on ρ_{xx} are both in agreement with previous reports [12] (see Fig. 1).

III. EXPERIMENTAL RESULTS

A. ρ_{xy} with magnetic field applied along the easy axis

Before addressing the change in ρ_{xy} due to changes in the orientation of **M**, we present $\rho_{xy}(\mathbf{B})$ at different temperatures with **B** along the easy axis (Fig. 2). We note that as the temperature decreases, the slope becomes less linear and eventually it changes its sign. This behavior is attributed to the low-temperature long mean free path in the sample with the high RRR. Films with smaller RRR do not exhibit such a behavior (see Fig. 2). The measurements shown below were performed in the temperature range where ρ_{xy} exhibits deviations from linearity in the relevant field range.

B. ρ_{xy} with magnetization tilted away from the easy axis

To identify magnetization-related contributions to ρ_{xy}, we have compared its value in states with the same **B** or $B_\perp$ but different angles ϕ between **M** and the film normal in the (001) plane. We have performed three types of experiments. In the first type, we have measured ρ_{xy} in a hysteresis loop with **B** at a fixed angle θ with respect to the film normal in the (001) plane, to compare ρ_{xy} with the same **B** in the ascending and descending branches. In the second type, we have measured ρ_{xy} for a fixed **B** as a function of θ. The sample was rotated clockwise and anticlockwise to compare ρ_{xy} for the same **B** in the two rotation branches. Both methods enable the comparison between two states with the same θ and two different values of ϕ. In the third type, we have compared measurements of ρ_{xy} for pairs of fields applied with the same angle relative to the film normal in the (001) plane on both

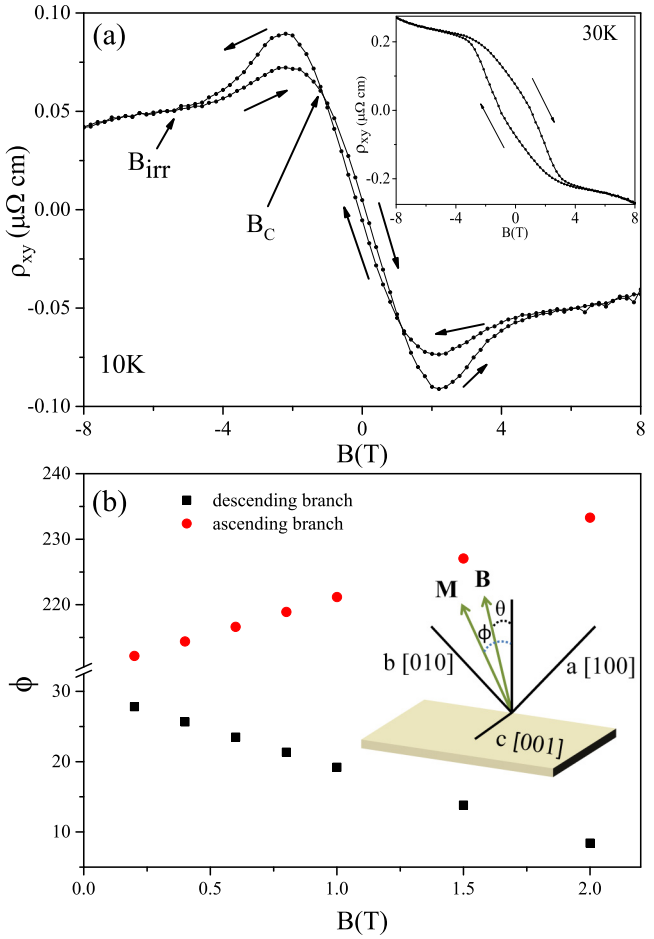

FIG. 3. (Color online) (a) ρ_{xy} vs **B** applied 5° from the hard axis (−55° from the film normal) at 10 K. Inset: ρ_{xy} vs **B** applied 5° from the hard axis at 30 K. The arrows indicate the field-sweeping direction. (b) The magnetization angle ϕ as a function of **B** in the ascending and descending branches in (a). The inset shows the angle θ (ϕ) between **B** (**M**) and the film normal.

sides of the film normal. In these measurements, $B_\perp$ is the same whereas ϕ is different.

1. ρ_{xy} with a magnetic field applied close to the hard axis in the (001) plane

The first types of measurements are presented in Fig. 3(a), which shows ρ_{xy}(**B**), where **B** is in the (001) plane 5° from the hard axis (the hard axis is at −60° from the film normal at the relevant temperature). A regular magnetization hysteresis loop [$M(B)$] closes at an "irreversibility" field ($B_{\rm irr}$) above which the magnetization is uniform and independent of field history. Below $B_{\rm irr}$, there are two branches, where the average magnetization in the decreasing field branch is more positive. HE hysteresis loops [ρ_{xy}(**B**)] are commonly proportional to the hysteresis loops of $M_\perp$ (the component of the magnetization that is perpendicular to the film plane) after the OHE contribution is subtracted, indicating that the AHE has a negligible field dependence and it is simply the sum of the contributions of all magnetic domains. Here, however, we obtain qualitatively different HE hysteresis loops.

Figure 3(a) exhibits a hysteresis loop at 10 K with the two branches intersecting. Loop crossing is observed only up to about 12 K. At higher temperatures, regular hysteresis loops are obtained [see inset of Fig. 3(a)] due to a decrease in $B_{\rm irr}$. We call the crossing point below $B_{\rm irr}$ the crossover field B_C. Above B_C, ρ_{xy} that corresponds to the decreasing field is higher, and the situation is reversed below B_C. Figure 3(b) shows the calculated ϕ in the two branches. Here and below, ϕ is calculated according to the Stoner-Wohlfarth model [18] using an anisotropy field of 7 T (see Ref. [19] for detail). The main observation is the sign change in the difference between ρ_{xy} in the ascending and descending branches.

2. ρ_{xy} with an applied magnetic field rotating in the (001) plane

The second type of measurements used to compare ρ_{xy} with the same **B** and different **M** are presented in Fig. 4. The figure shows the dependence of ρ_{xy} on θ for $B = 5$ T at $T = 5$ K. The inset of Fig. 4(a) shows ϕ as a function of θ for different applied fields. The easy axis at the relevant temperatures is 30° from the film normal in the (001) plane, and the hard axis is 120° degrees from the film normal in the same plane. We note that the sharp changes in $\rho_{xy}(\theta)$ correspond to sharp changes in ϕ for θ in the vicinity of the hard axis where magnetization reversal occurs. Because of these sharp changes, instead of

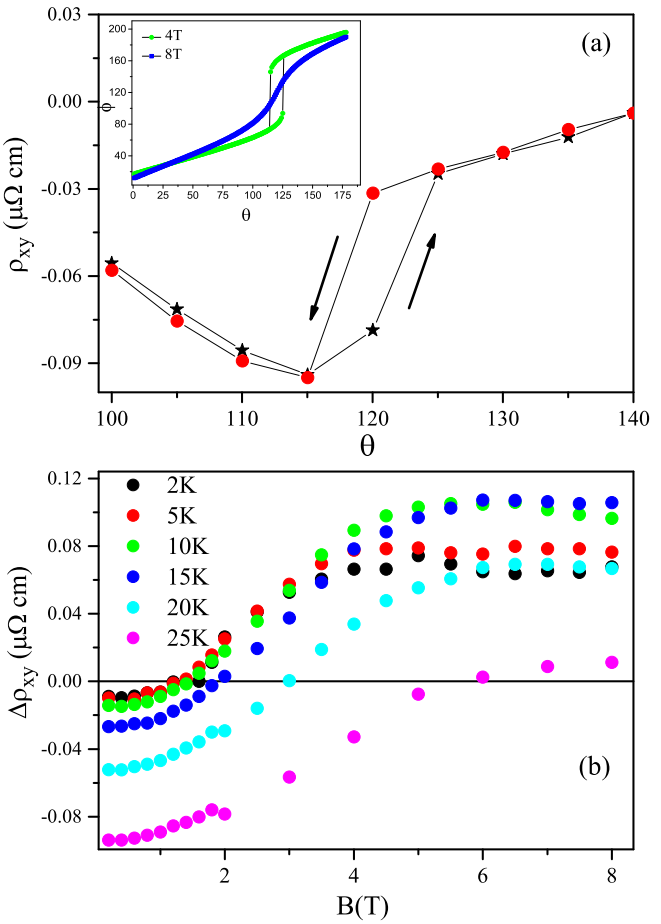

FIG. 4. (Color online) (a) ρ_{xy} vs θ, $T = 5$ K, and $B = 5$ T. Inset: ϕ vs θ for two fields. The arrows indicate the angular sweeping direction. (b) $\Delta\rho_{xy}$ vs B at different temperatures.

comparing ρ_{xy} when the field is along the hard axis for the two rotation branches, we prefer to extrapolate $\rho_{xy}(\theta)$ from both sides of the hard axis from the slowly varying regions of ρ_{xy} and define $\Delta\rho_{xy}(B)$ as the extrapolated difference between ρ_{xy} when the field is along the hard axis for states with opposite corresponding remanent magnetization. Figure 4(b) shows $\Delta\rho_{xy}(B)$ for different temperatures. The main observation is the sign change of $\Delta\rho_{xy}$ above a threshold field and the values that $\Delta\rho_{xy}$ obtains at higher fields, which are an order of magnitude larger than ρ_{xy} at zero field.

3. ρ_{xy} with a magnetic field applied at different angles in the (001) plane

Figure 5 shows the third type of experiments, which demonstrate the large deviation in ρ_{xy} due to changes in the orientation of **M**. It shows ρ_{xy} with **B** applied at different angles relative to the film normal in the (001) plane as a function of $B_\perp$. In particular, we notice pairs of measurements where the field is applied at equal angles on both sides of the film normal in the (001) plane. For such pairs, the perpendicular component of the field, expected to determine the OHE, is the same. What is clearly observed is that the differences between the curves

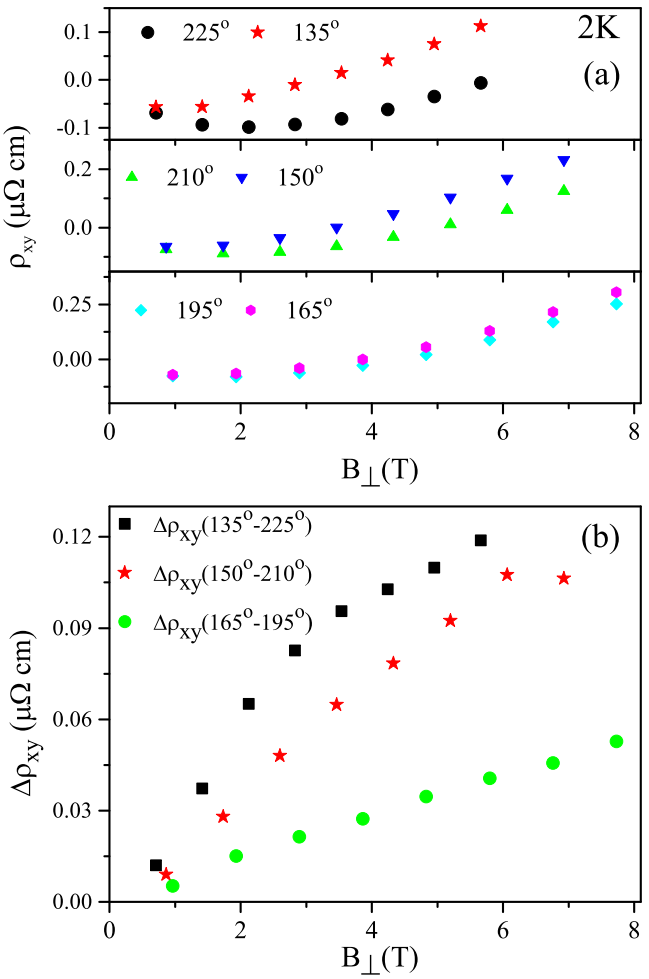

FIG. 5. (Color online) (a) ρ_{xy} vs $B_\perp$ for different values of θ (indicated in the legend) at 2 K. (b) The difference in ρ_{xy} for pairs of measurements with the same angle with respect to the film normal (see the legends) vs $B_\perp$ at 2 K.

of such pairs are more than an order of magnitude higher than the spontaneous AHE.

IV. DISCUSSION

The measurements presented above clearly indicate dramatic changes in ρ_{xy} associated with changes in the orientation of **M**. Therefore, we start by addressing the question of whether it is possible to describe the obtained results assuming ρ_{xy} is a combination of an OHE contribution that depends on $B_\perp$ and an AHE contribution that depends on **M**. In this scenario, when **B** is along the easy axis ($\theta = \theta_{\rm EA}$) and the temperature is sufficiently low, the AHE is practically field-independent, as both the direction and magnitude of **M** do not change. Thus, these measurements can be used to determine the assumed OHE contribution as a function of $B_\perp$. When **B** is not along the easy axis, we define $\Delta^*\rho_{xy}(B,\theta) = \rho_{xy}(B,\theta) - \rho_{xy}(\tilde{B},\theta_{\rm EA}) - \rho_{xy}(B=0)$, where $B_\perp = \tilde{B}_\perp$. With the assumptions we made, $\Delta^*\rho_{xy}(B,\theta)$ is the change in ρ_{xy} associated with the change in ϕ. Based on the data presented in Fig. 5, we present in Fig. 6 the extracted value of $\Delta^*\rho_{xy}$ as a function of ϕ. Clearly, there is no scaling, and this is also the case if some variations in the anisotropy field are allowed. Namely, the results strongly suggest that the AHE is affected by **B** also directly and not merely due to its effect on the magnetization.

A possible interpretation of these observations is that the magnetic field induces changes in the band structure of $SrRuO_3$, most prominently by altering the position of Weyl nodes [10,11]. As shown in Ref. [11], the AHE in a ferromagnetic Weyl metal includes a universal contribution proportional to the k-space distance between Weyl nodes, which is dictated by the exchange-enhanced Zeeman splitting. As a result, a continuous tuning of **B** directly alters this component of the AHE via the effective magnetic field $\mathbf{B}_{\rm eff}$, which couples to the spin. Due to the anisotropy of magnetism in this material, $\mathbf{B}_{\rm eff}$ depends on both the magnitude and orientation of **B**, and these cannot be easily disentangled. To be concrete, assuming a mean-field solution of a Heisenberg ferromagnet with anisotropic exchange constants J_e, J_h in

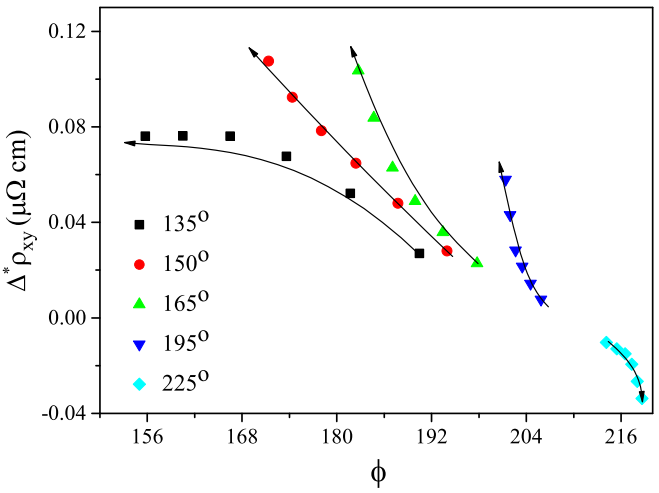

FIG. 6. (Color online) $\Delta^*\rho_{xy}$ defined in the text vs ϕ for different angles at which the field is applied (see the legends). The arrows indicate increasing fields between 2 and 8 T at 2 K.

the easy- and hard-axis directions, respectively ($J_e > J_h$), the effective Zeeman field is given by

$$\mathbf{B}_{\text{eff}} = \left(B\cos\tilde{\theta} + \frac{J_e}{g\mu_B}\cos\tilde{\phi}\right)\hat{\mathbf{e}} + \left(B\sin\tilde{\theta} + \frac{J_h}{g\mu_B}\sin\tilde{\phi}\right)\hat{\mathbf{h}}; \quad (1)$$

here g is an effective g-factor, $\tilde{\phi}$ and $\tilde{\theta}$ denote the tilt angles of $\mathbf{M}$ and $\mathbf{B}$ with respect to the easy axis, and $\hat{\mathbf{e}}$ and $\hat{\mathbf{h}}$ are unit vectors in the direction of the easy and hard axes. It is apparent from Eq. (1) that the magnitude as well as the orientation of $\mathbf{B}_{\text{eff}}$ are nontrivially dependent on $\mathbf{B}$, both explicitly and implicitly due to its effect on $\tilde{\phi}$. The resulting effect on the band structure is further complicated by the tilting of the easy axis $\hat{\mathbf{e}}$ by an angle θ_{EA} with respect to the normal to the sample plane, which dictates the spin component dominating the AHE. The projection of $\mathbf{B}_{\text{eff}}$ on this direction is

$$\mathbf{B}^z_{\text{eff}} = B(\cos\theta_{\text{EA}}\cos\tilde{\theta} - \sin\theta_{\text{EA}}\sin\tilde{\theta}) + \frac{J_e}{g\mu_B}\cos\theta_{\text{EA}}\cos\tilde{\phi} - \frac{J_h}{g\mu_B}\sin\theta_{\text{EA}}\sin\tilde{\phi}. \quad (2)$$

Note that this expression includes terms that change sign when $\tilde{\theta}$ (and hence also $\tilde{\phi}$) are tuned across the easy-axis direction $\tilde{\theta} = \tilde{\phi} = 0$. This behavior is consistent with the sign reversal of $\Delta^*\rho_{xy}$ across the easy axis (see Fig. 6). In addition, we note that the magnitude of B_{eff}, which determines the effective Zeeman splitting, is particularly sensitive to the magnetic orientation when the magnitude of B becomes comparable to the anisotropy scale, i.e., for $g\mu_B B \sim (J_e - J_h)$. Indeed, the estimated anisotropy in $SrRuO_3$ is Ref. [15] $(J_e - J_h) \approx 0.3J_{\text{av}}$ equivalent to $B \sim 7$ T. This feature is qualitatively consistent with the experimental results, which show large changes in the HE associated with changes in magnetic orientation.

V. CONCLUSIONS

We measured the HE in exceptionally high-quality films of $SrRuO_3$ and found unusually large changes in the HE associated with changes in magnetic orientation. To study the effect of magnetic orientation on the HE, we have performed three types of measurements: (a) ρ_{xy} versus magnetic field applied close to the hard axis in the (001) plane, (b) ρ_{xy} versus the orientation of a magnetic field applied in the (001) plane, and (c) ρ_{xy} versus magnetic field for pairs of symmetric orientations in the (001) plane on both sides of the film normal. The first two types of measurements enabled a comparison of ρ_{xy} for two states with the same applied magnetic field and different magnetic orientation. The third type of measurements enabled a comparison of ρ_{xy} for pairs of states with the same perpendicular component of the applied magnetic field and different magnetic orientation. The three types of experiments clearly demonstrate that changes in ρ_{xy} associated with changes in the magnetic orientation are more than an order of magnitude larger than the spontaneous AHE. In addition, our attempt to scale some of our data, assuming the HE is a sum of a term that depends on the magnetic field and a term that depends on the magnetization, was unsuccessful, which strongly indicates that the OHE and the AHE are effectively intermixed. What makes these intriguing observations even more exciting are previous calculations of the band structure of $SrRuO_3$ that indicated the existence of Weyl nodes whose expected effect on the AHE is qualitatively consistent with our experimental observations.

ACKNOWLEDGMENTS

L.K. acknowledges support by the U.S.-Israel Binational Science Foundation (2012169) and by the Israel Science Foundation founded by the Israel Academy of Sciences and Humanities (703/11). E.S. acknowledges support by the U.S.-Israel Binational Science Foundation (2012120) and by the Israel Science Foundation founded by the Israel Academy of Sciences and Humanities (231/14). We are grateful to Anton Burkov for useful discussions and comments on the manuscript. J.W.R. grew the samples at Stanford University in the laboratory of M. R. Beasley.

[1] X. Qi and S. Zhang, Phys. Today **63**(1), 33 (2010).
[2] L. Balents, Physics **4**, 36 (2011); X. Wan, A. M. Turner, A. Vishwanath, and S. Y. Savrasov, Phys. Rev. B **83**, 205101 (2011).
[3] N. Nagaosa, J. Sinova, S. Onoda, A. H. MacDonald, and N. P. Ong, Rev. Mod. Phys. **82**, 1539 (2010).
[4] J. Smit, Physica **21**, 877 (1955); **24**, 39 (1958).
[5] L. Berger, Phys. Rev. B **2**, 4559 (1970); **5**, 1862 (1972).
[6] R. Karplus and J. Luttinger, Phys. Rev. **95**, 1154 (1954).
[7] Y. Yao, L. Kleinman, A. H. MacDonald, J. Sinova, T. Jungwirth, D. S. Wang, E. Wang, and Q. Niu, Phys. Rev. Lett. **92**, 037204 (2004).
[8] T. Jungwirth, Q. Niu, and A. H. MacDonald, Phys. Rev. Lett. **88**, 207208 (2002).
[9] Z. Fang, N. Nagaosa, K. S. Takahashi, A. Asamitsu, R. Mathieu, T. Ogasawara, H. Yamada, M. Kawasaki, Y. Tokura, and K. Terakura, Science **302**, 92 (2003).
[10] Y. Chen, D. L. Bergman, and A. A. Burkov, Phys. Rev. B **88**, 125110 (2013).
[11] A. A. Burkov, Phys. Rev. Lett. **113**, 187202 (2014).
[12] N. Haham, Y. Shperber, M. Schultz, N. Naftalis, E. Shimshoni, J. W. Reiner, and L. Klein, Phys. Rev. B **84**, 174439 (2011); N. Haham, J. W. Reiner, and L. Klein, *ibid.* **86**, 144414 (2012).
[13] M.-H. Kim, G. Acbas, M.-H. Yang, M. Eginligil, P. Khalifah, I. Ohkubo, H. Christen, D. Mandrus, Z. Fang, and J. Cerne, Phys. Rev. B **81**, 235218 (2010).
[14] G. Koster, L. Klein, W. Siemons, G. Rijnders, J. S. Dodge, C.-B. Eom, D. H. A. Blank, and M. R. Beasley, Rev. Mod. Phys. **84**, 253 (2012).

[15] Y. Kats, I. Genish, L. Klein, J. W. Reiner, and M. R. Beasley, Phys. Rev. B **71**, 100403(R) (2005).
[16] L. Klein, J. S. Dodge, C. H. Ahn, J. W. Reiner, L. Mieville, T. H. Geballe, M. R. Beasley, and A. Kapitulnik, J. Phys. Condens. Matter **8**, 10111 (1996).
[17] M. Buttiker, Phys. Rev. Lett. **57**, 1761 (1986).
[18] E. C. Stoner and E. P. Wohlfarth, Philos. Trans. R. Soc. London, Ser. A **240**, 599 (1948).
[19] N. Haham, Y. Shperber, J. W. Reiner, and L. Klein, Phys. Rev. B **87**, 144407 (2013).